HHS Public Access

Author manuscript

Circ Cardiovasc Imaging. Author manuscript; available in PMC 2018 May 01.

Published in final edited form as:

Circ Cardiovasc Imaging. 2017 May ; 10(5): . doi:10.1161/CIRCIMAGING.116.005813.

Atheroma Susceptible to Thrombosis Exhibit Impaired Endothelial Permeability In Vivo as Assessed by Nanoparticle-Based Fluorescence Molecular Imaging

Ashley F. Stein-Merlob, MD[1], **Tetsuya Hara, MD PhD**[1], **Jason R. McCarthy, PhD**[2], **Adam Mauskapf, BS**[1], **James A. Hamilton, PhD**[3], **Vasilis Ntziachristos, PhD**[4], **Peter Libby, MD**[5], and **Farouc A. Jaffer, MD PhD**[1]

[1]Cardiovascular Research Center, Massachusetts General Hospital, Harvard Medical School, Boston, MA

[2]Center for Systems Biology, Massachusetts General Hospital, Harvard Medical School, Boston, MA

[3]Department of Physiology and Biophysics, Boston University School of Medicine, Boston MA, Department of Biomedical Engineering, Boston University, Boston MA

[4]Institute of Biological and Medical Imaging, Technical University of Munich, Munich, Germany

[5]Cardiovascular Division, Brigham and Women's Hospital, Harvard Medical School, Boston, MA

Abstract

Background—The role of local alterations in endothelial functional integrity in atherosclerosis remains incompletely understood. This study utilized nanoparticle-enhanced optical molecular imaging to probe in vivo mechanisms involving impaired endothelial barrier function in experimental atherothrombosis.

Methods and Results—Atherosclerosis was induced in rabbits (n=31) using aortic balloon injury and high-cholesterol diet. Rabbits received ultrasmall superparamagnetic iron oxide nanoparticles (CLIO) derivatized with a near-infrared fluorophore (CyAm7) 24 hours before near-infrared fluorescence (NIRF) imaging. Rabbits were then either sacrificed (n=9) or underwent a pharmacologic triggering protocol to induce thrombosis (n=22). CLIO-CyAm7 nanoparticles accumulated in areas of atheroma ($p<0.05$ vs. reference areas). On NIRF microscopy, CLIO-CyAm7 primarily deposited in the superficial intima within plaque macrophages, endothelial cells and smooth muscle cells. Nanoparticle-positive areas further exhibited impaired endothelial barrier function as illuminated by Evans blue leakage. Deeper nanoparticle deposition occurred in areas of plaque neovascularization. In rabbits subject to pharmacological triggering, plaques that thrombosed exhibited significantly higher CLIO-CyAm7 accumulation compared to non-thrombosed plaques ($p<0.05$). In thrombosed plaques, nanoparticles accumulated preferentially at the plaque-thrombus interface. Intravascular two-dimensional NIRF imaging detected nanoparticles in human coronary-sized atheroma in vivo ($p<0.05$ vs. reference segments).

Corresponding Author: Farouc Jaffer MD PhD, MGH CVRC, 185 Cambridge Street, Simches Research Building, Room 3206, Boston, Massachusetts 02114, fjaffer@mgh.harvard.edu, Tel. (617) 724-9353, Fax. (617) 860-3180.

Conclusions—Plaques that exhibit impaired in vivo endothelial permeability in cell-rich areas are susceptible to subsequent thrombosis. Molecular imaging of nanoparticle deposition may help to identify biologically high-risk atheroma.

Keywords

atherosclerosis; thrombosis; molecular imaging; intravascular imaging; endothelium

The majority of acute coronary syndromes (ACS) result from focal thrombosis complicating atherosclerotic plaques. Achieving an understanding of rupture of the plaque's fibrous cap has dominated thinking about the underlying mechanisms of coronary thrombosis.[1] However, post-mortem human studies of coronary vessels by histology have found that majority of plaques with thin fibrous caps did not disrupt.[2] Furthermore, plaque rupture is diminishing as a cause of ACS, likely due to statin treatment and other preventive measures. Therefore, alterations in endothelial functions merit further scrutiny, particularly given the dearth of mechanistic information regarding mechanisms of superficial erosion and subsequent plaque thrombosis.[3] Although many studies have addressed endothelial vasodilator function in vivo, investigation of other aspects of local endothelial integrity and its role in atherothrombosis has lagged.

This study tested the hypothesis that plaques exhibiting impaired in vivo endothelial barrier function (abnormal permeability) would be predisposed to plaque thrombosis. We further hypothesized that plaque susceptibility to thrombosis would relate to areas of high atheroma cell density, as plaque cells are often pro-inflammatory and can amplify endothelial cell dysfunction.[4] To test these hypotheses, we engineered and applied CLIO-CyAm7, a near-infrared fluorophore (NIRF) derivatized-ultrasmall superparamagnetic iron oxide (USPIO) nanoparticle, to assess experimental atherosclerosis biology in vivo. We first assessed the cellular distribution of the fluorescent USPIO in rabbit atheroma, and found that its cellular targeting profile appeared diffusion limited. This finding motivated us to investigate whether an impaired endothelial barrier function might govern CLIO-CyAm7 nanoparticle deposition into atheroma. Next, to understand the relationship between nanoparticle deposition and plaque thrombosis, we employed a modified procedure developed by Constantinides to trigger thrombosis[5–7] to assess whether sites of mural thrombosis accumulated CLIO-CyAm7. Lastly we analyzed the ability of CLIO-CyAm7 nanoparticles to enable intravascular NIRF molecular imaging of impaired endothelial barrier function in vivo in coronary-sized arteries.

METHODS

Please see the Supplement for an expanded methods section.

Animal Model of Atherothrombosis

Animal protocols were approved by the Massachusetts General Hospital Subcommittee on Research Animal Care. New Zealand white rabbits (n=31) consumed a high cholesterol diet (HCD) for two weeks before abdominal aortic balloon injury followed by six weeks of 1% HCD and four weeks of normal chow (Supplemental Figure 1).[5, 6]

CLIO-CyAm7 studies of rabbit atherosclerosis and triggered atherothrombosis

Rabbits with atheroma underwent intravenous injection of NIR fluorescent USPIO nanoparticles (n=21, CLIO-CyAm7 group, Supplemental Figure 2) or saline (n=3) at the end of the preparation protocol. Rabbits were sacrificed at 24 hours or underwent two rounds of thrombosis triggering twenty-four hours apart with Russell's viper venom (0.15 mg/kg IP, Sigma Chemical Co) followed 30 minutes later by histamine (0.02 mg/kg IV, Sigma Chemical Co). Rabbits underwent intravascular NIRF and ultrasound (IVUS) imaging during the double triggering protocol (Supplemental Figure 1). A subgroup of rabbits (n=7) also underwent assessment for impaired endothelial permeability assessed by Evans Blue dye leakage (6 mL intravenous injection 0.5%, Sigma Chemical Co.) 30 minutes before sacrifice.[8] A higher dose of CLIO-CyAm7 (5.0 mg/kg) was used in these rabbits to overcome partial fluorescence overlap with Evans Blue.

In Vivo intra-arterial NIRF molecular imaging and IVUS structural imaging

Intravascular two-dimensional NIRF molecular imaging—Prior to pharmacologic triggering, 15 rabbits underwent *in vivo* intravascular NIRF imaging of CLIO-CyAm7 deposition using a custom-built standalone 2D NIRF catheter-based system (750nm laser excitation).[9] Four 90–100 mm pullbacks from the iliac bifurcation to the renal arteries were performed through blood, without flushing.[9, 10] The peak target-to-background ratio (TBR) was calculated for regions of atheroma across all pullbacks (MATLAB R2011a MathWorks). Regions with a luminal diameter of greater than 5 mm were excluded due to NIR light attenuation.

IVUS Structural assessment of atherosclerosis and atherothrombosis—IVUS images (Galaxy IVUS System, Boston Scientific) interrogated atheroma structure before triggering, and then after triggering to identify large luminal thrombi. IVUS images were co-registered to NIRF images using radiopaque markers on x-ray angiography. IVUS pre- and post-triggering images were co-registered to each other using side branches as fiducial markers.

Analysis of CLIO-CyAm7 Nanoparticle Distribution in Atheroma and Atherothrombosis

After sacrifice, rabbits underwent fluorescence reflectance imaging (FRI), fluorescence microscopy, and histopathology analyses to determine the distribution of CLIO-CyAm7 nanoparticles in atheroma (NIH ImageJ). The percent positive CLIO-CyAm7 pixels were calculated in the superficial 100μm of uniformly thresholded fluorescence microscopy images. In sections from rabbits injected with Evans Blue, the maximum distance from the luminal plaque surface to either the deepest CLIO-CyAm7 signal, or Evans Blue signal, or internal elastic membrane (plaque thickness) were measured. Correlation coefficients were calculated to determine the relationship between these depths. See Supplement for details.

Statistical Analysis

For all analyses between two groups, nonparametric Mann-Whitney U test was used (GraphPad Prism v5.0, San Diego, CA). Thresholds for specificity and sensitivity

calculations were determined using an ROC curve optimization. Data are presented as mean ± standard deviation or 95% confidence intervals (CI).

RESULTS

CLIO-CyAm7 nanoparticles localize to the luminal surface of atheroma

While ultrasmall superparamagnetic iron oxide nanoparticles are well-established cellular MRI reporters for atherosclerosis,[11–13] their precise cellular and topographical distribution in coronary artery-sized atheroma is incompletely understood. NIRF nanoparticles allowed assessment of USPIO uptake in rabbit atheroma using fluorescence imaging (Figures 1,2). *Ex vivo* macroscopic and microscopic NIR fluorescence imaging illuminated plaque areas with high CLIO-CyAm7 uptake (Figure 1A). In contrast, minimal NIRF signal emerged in control rabbits receiving saline (Figure 1B), in accord with prior results.[9, 14–16] Aortic atheroma exhibited increased CLIO-CyAm7 nanoparticle signal compared to control areas (Figure 1C, SNR 18.1±11.3 versus 10.64±1.2 in the uninjured renal artery, p=0.03). On fluorescence microscopy, CLIO-CyAm7 primarily accumulated in the superficial intima, with a smaller component in deeper plaque regions (Figures 1D,E, Figure 2). CLIO-CyAm7 deposition was not uniform circumferentially across the atheroma surface (Figure 1D). Fluorescence microscopic analysis of the superficial intima demonstrated increased CLIO-CyAm7+ deposition in atheroma compared to the uninjured aorta (Figure 1F, 1.73±1.9% vs. 0.13±0.28%, $p<0.0001$).

Cellular distribution of iron oxide nanoparticles in atheroma

USPIO nanoparticles appear to localize primarily in macrophages in atheroma,[11, 17, 18] but detailed assessment of USPIO localization in other atheroma cells is limited. We therefore examined the cellular localization of CLIO-CyAm7 within plaque macrophages (Figure 2 A2), SMCs (Figure 2 A3) and endothelial cells (Figure 2 A1), and found evidence of CLIO-CyAm7 deposition within each of these three cell types (Figure 2). Analysis of representative sections from each triggered rabbit demonstrated restriction of the CLIO-CyAm7 signal to the luminal plaque surface in the majority of rabbits (67%), despite the presence of numerous cells deeper within the atheroma (Figure 2A). This observation suggested that restricted diffusion could also govern nanoparticle deposition.

The remaining 33% of rabbits showed evidence of deeper CLIO-CyAm7 deposition at the intimal-medial border (Figure 2B). CD31 staining for endothelial cells showed evidence of neovascularization in these deeper regions, providing a plausible access route for nanoparticles to deposit more deeply into atheroma. Although CLIO-CyAm7 localized near the CD31+ neovasculature (Figure 2 B1), CLIO-CyAm7 signal did not localize to CD31+ cells, but rather targeted nearby macrophages identified by RAM11 staining (Figure 2 B2).

CLIO-CyAm7 deposits in areas of impaired endothelial permeability

Evidence of heterogeneous CLIO-CyAm7 distribution across the atheroma surface (Figure 1D) and within areas of neovascularization (Figure 2B) indicated that CLIO-CyAm7 deposition could relate to regional alterations in endothelial permeability. We therefore tested this hypothesis by co-injecting Evans Blue, a fluorescent azo dye that binds albumin.

Evans blue deposition in the intima indicates increased, abnormal endothelial permeability.[16, 19] Following co-injection of Evans Blue in rabbits injected with CLIO-CyAm7, atheroma exhibited varying degrees of Evans Blue uptake (Figure 3). The depth of Evans Blue fluorescence signal in plaques correlated well with the depth of CLIO-CyAm7 penetration (r=0.64, p=0.003, Figure 3E). The depth of Evans blue penetration however did not relate to the overall plaque thickness (r=0.12, p=0.61, Figure 3D,F).

In vivo NIRF molecular imaging of CLIO-CyAm7 deposition

In vivo detection of CLIO-CyAm7 nanoparticle deposition in atheroma could offer an approach to detect biologically-high risk plaques. Further experiments therefore investigated whether CLIO-CyAm7 could provide sufficient signal to enable intravascular NIRF imaging of atheroma in vivo. Intravascular NIRF imaging is a high-resolution approach emerging for molecular imaging of coronary artery-sized vessels.[20–22] Multimodality imaging, including x-ray angiography, 2D NIRF, and IVUS imaging, was performed before triggering (Figure 4A,B,C respectively, N=15 rabbits). Intravascular NIRF imaging performed through blood[9] demonstrated the ability to detect NIRF nanoparticle signal in areas of IVUS-confirmed atheroma (Figure 4B,C).

After pharmacological triggering with Russell's viper venom and histamine to induce atherothrombosis, follow-up IVUS imaging at 48 hours revealed new luminal thrombi overlying areas of atheroma (Figure 4C,D). The average luminal diameter as measured by IVUS was 3.41±0.78mm (range 1.93mm–5.87mm), with some animals developing aneurysms (Figure 4G). Of note multiple segments were larger than the typical 2.5–3.5 mm diameter of human coronary arteries to which the intravascular NIRF system is optimally calibrated.[9] Ex vivo FRI at 72 hours after initial CLIO-CyAm7 injection still detected CLIO-CyAm7 in atheroma (Figure 4F). Atheroma generated a significantly higher peak TBR compared to the uninjured control aorta (peak TBR 2.86±1.82 vs. 1.55±0.65, p=0.001, respectively, Figure 4H; Supplemental Figure 3).

CLIO-CyAm7 nanoparticle deposition underlies areas of plaque thrombosis in vivo and by histological analysis

Ten of fifteen rabbits (67%) undergoing pharmacological triggering developed plaque thrombosis as confirmed by histologic examination (Figure 5). A total of 21 of 51 atheroma segments compiled from all rabbits exhibited adherent thrombus (41%) on Carstairs' staining. In vivo IVUS images demonstrated thrombus in 4 out of 9 rabbits with confirmation on Carstairs' stain following sacrifice. IVUS-detectable thrombi were larger than those identified by Carstairs' alone (4.4±5.0μm^2 vs. 0.42±0.39μm^2), suggesting that IVUS had lower sensitivity to detect smaller thrombi.

Quantitative analysis revealed that the 21 plaques with adherent Carstairs'-positive thrombus exhibited higher CLIO-CyAm7 accumulation than the 30 plaques without thrombus (Figure 5C, 2.1±1.7% vs. 1.5±1.9%, respectively, p=0.045). CLIO-CyAm7 nanoparticles abutted thrombi, particularly at plaque shoulders (Figure 5D,5G). Receiver operator curve (ROC) analysis determined that the optimal threshold for CLIO-CyAm7 positivity on fluorescence microscopy was 0.85% positive area (Supplemental Figure 4). This threshold provided a

sensitivity and specificity of 82.6% (CI 61.2% to 95%) and 61.8% (CI 43.6% to 77.8%) respectively for plaque thrombosis. Utilizing this threshold criterion, the positive predictive value of a CLIO-positive plaque for plaque thrombosis was 59.4% (CI 40.6% to 76.3%), and the negative predictive value was 84.0% (CI 63.9% to 95.4%).

DISCUSSION

Atherosclerosis progression and plaque destabilization involves the interplay between multiple cell types including macrophages, endothelial cells, and SMCs. This study investigated the role of impaired endothelial permeability and atheroma cell distribution by assessing the distribution of NIR fluorescent CLIO-CyAm7 nanoparticles[12, 17] in experimental atherothrombosis. The overall results demonstrate that plaques that exhibit impaired endothelial permeability and surface atheroma cellularity have heightened susceptibility to subsequent thrombosis. From an imaging standpoint, the current data sharpens the understanding of nanoparticle targeting in atheroma. USPIO nanoparticles can deposit in all major atheroma cell types and specifically in areas of impaired endothelial permeability, as supported by Evans Blue deposition and neovessel presence. In addition, CLIO-CyAm7 enables intravascular NIRF imaging of various atheroma cell types and altered endothelial permeability in vivo through blood, offering the potential for translational detection of biologically high-risk plaques.

Despite evaluation of USPIO in several experimental and clinical atherosclerosis studies, the precise targeting profile of USPIO nanoparticles in atherosclerosis is incompletely understood. The current investigation leveraged the engineered fluorescence capabilities of the CLIO-CyAm7 USPIO nanoparticle and examined over 50 plaques in the rabbit aorta, a vessel of similar caliber as human coronary arteries. While USPIOs are established macrophage reporter agents, non-macrophage cells might also contribute to USPIO retention in atherosclerosis.[19, 23–25] This study confirmed that USPIOs could not only target plaque macrophages, but also target some peri-luminal plaque SMCs and intimal endothelial cells. SMCs undergo phenotypic changes in the inflammatory milieu of the atherosclerotic plaque.[26–28] Lesional SMCs bear adhesion molecules, class II major histocompatibility molecules, and tissue factor, indicating inflammatory activation and the potential to drive atherothrombosis.[26, 28–33] Inflammatory SMCs can thus phagocytose CLIO-CyAm7 given its similar size compared to LDL.[25, 34] In this regard, the nanoparticle preparation ferumoxtran, a clinical analog of CLIO, can localize within cells with both SMC- and macrophage-like characteristics on electron microscopy.[17, 24] The overall findings extend prior work by showing that USPIO nanoparticles accumulate in macrophages, pathologic endothelial cells and inflammatory SMCs.[19, 24, 34–36]

This study demonstrated that USPIO nanoparticle deposition was heterogeneous, even across a plaque's circumference (Figure 1D). Histological analyses revealed that CLIO-CyAm7 deposited primarily within the first 100 micrometers of the plaque surface, despite abundant plaque cells, including macrophages, throughout deeper regions of the plaques. The heterogeneous distribution of CLIO nanoparticles in atheroma suggested that altered endothelial permeability in atherosclerosis could modulate nanoparticle deposition, a phenomenon identified in cancer studies as the enhanced permeability and retention (EPR)

effect.[37] This hypothesis was confirmed when Evans blue deposition identified impaired endothelial permeability consistently in areas of CLIO-CyAm7 deposition. The depth of Evans Blue stain further correlated with the depth of CLIO-CyAm7 penetration, indicating that enhanced plaque permeability tracked with impaired endothelial permeability (Figure 3).

These results provide evidence that impaired endothelial barrier function, often but variably present in atherosclerosis, links to USPIO deposition in atheroma. These findings parallel those in arteriovenous fistulae that also exhibit pathological endothelial permeability,[19] and is further supported by CLIO-CyAm7 accumulation in deeper plaque macrophages adjacent to areas of microvascular CD31+ endothelial cells (Figure 2B). Neovascularization, the growth of the vasa vasorum from the adventitia to the media and eventually in the deep intima, promotes intraplaque hemorrhage due to the fragile, leaky neovessels and increases the risk of plaque rupture.[38] Thus, USPIO nanoparticle localization in the atheroma intima and regions of neovascularization illuminates impaired endothelial barrier function in atherosclerosis. This capability might also have future application to assess superficial plaque erosion, a mechanism of coronary thrombosis of increasing interest in the current era.[3]

Attesting to the important pathological consequences of impaired endothelial barrier function and atheroma pro-inflammatory cells, plaques that developed triggered thrombosis showed enhanced USPIO nanoparticle uptake (Figure 5H). Nanoparticle deposition further occurred at plaque shoulders, areas associated with plaque disruption and subsequent thrombosis. These findings suggest that USPIO nanoparticles distinguish specific atheroma and even regions of atheroma prone to develop thrombosis, and imaging of USPIO deposition might prove useful in enhancing subject-specific and plaque-specific risk of atherothrombotic events.

Alternative approaches to detect impaired endothelial permeability include dynamic contrast-enhanced MRI using albumin-binding contrast agents,[6, 8, 39, 40] or indocyanine green-based NIRF imaging.[15, 16] Comparatively, CLIO-CyAm7 may provide more durable cellular uptake, including into macrophages, endothelial cells and smooth muscle cells, and therefore can also serve as a reporter of cellular inflammation. Compared to MRI approaches, which have enabled clinical molecular MRI of inflamed carotid plaques[12, 17], higher resolution imaging approaches appear necessary for coronary artery imaging.[20–22] In a translational substudy, we leveraged the NIRF capabilities of the CLIO-CyAm7 USPIO to perform intravascular NIRF imaging, a clinically emerging approach for high-resolution imaging of human coronary arteries.[20–22, 41–43] *In vivo* NIRF imaging of CLIO-CyAm7 deposition in coronary-sized vessels demonstrated significantly higher NIRF signal in rabbit aortic plaques than control areas. The results demonstrate a new capability of NIRF imaging to assess atheroma cellularity and due to impaired endothelial barrier function in vivo. The current intravascular NIRF imaging results have promising clinical applicability, as NIR fluorophores,[15, 44] USPIOs,[12, 17] and intracoronary NIRF imaging[42] are clinically translatable.

This study has certain limitations. While triggering often provoked the formation of adherent thrombi, these sites rarely displayed plaque rupture characterized by a disrupted fibrous cap, a potential difference with human atherothrombosis, although plaque rupture has been previously described following this pharmacologic triggering procedure.[45–47] On the other hand, this finding of mural thrombosis at sites of defective endothelial barrier function enhances the relevance of the present findings to superficial erosion, an increasingly recognized cause of acute coronary syndromes. These results further agree with the findings on thrombosed lesions observed in myocardial infarction-prone atherosclerotic rabbits treated with a spasmogenic triggering regimen.[48] Higher-resolution confocal microscopic colocalization of CLIO-CyAm7 nanoparticles with cell-specific fluorescence antibodies was not possible, as commercial confocal systems are not equipped with 750nm range lasers; we therefore utilized epifluorescence colocalization approaches. Finally, *in vivo* fluorescence reflectance imaging is limited in a distance dependent manner as described previously, resulting in semi-quantitative NIRF signal assessment.[9] NIRF imaging has limited depth sensing, and therefore atheroma within aneurysmal segments (e.g. 5.0mm diameter, larger than a typical coronary artery) did not produce detectable in vivo NIRF signal. Since completion of this study, a combined OCT-NIRF catheter became available for integrated molecular-structural imaging,[49] however OCT signal detection requires saline-flushing, unlike the current standalone NIRF approach performed through flowing blood, without flushing.

In conclusion, this study demonstrates that USPIO nanoparticles deposit in plaque macrophages, SMCs and ECs associated with zones of impaired surface endothelial permeability as well as zones of neovascularization. Nanoparticle deposition further occurs in plaques that progress to thrombosis. These results shed new mechanistic light into the pathophysiology of the thrombotic complications of atherosclerosis. Further, intravascular imaging of NIR fluorescent nanoparticles may provide a novel translational approach to detect biologically high-risk plaques *in vivo*.

Supplementary Material

Refer to Web version on PubMed Central for supplementary material.

Acknowledgments

We thank Dr. George Mallas for assistance with intravascular 2D NIRF imaging and Dr. Lang Wang for performing additional control experiments.

Sources of Funding

NIH R01HL108229 and R01HL122388 (F.A.J) and HL080472 (P.L.), American Heart Association grants #12PRE11160000 (A.F.S); #13POST14640021 (T.H.); #13GRNT17060040 (F.A.J), Deutsche Forschungsgemeinschaft (DFG) as part of the CRC 1123 (Z1) (V.N.), and the Kanae Foundation for Research Abroad (T.H.).

Disclosures

Dr. Libby has had sponsored research grants from General Electric, GlaxoSmithKline, and Novartis. Dr. Jaffer has sponsored research grants from Kowa, Siemens, and Canon, has a consulting agreement with Boston Scientific and Abbott Vascular. Massachusetts General Hospital has a patent licensing arrangement with Canon Corporation, and Dr. Jaffer has the right to receive licensing royalties.

References

1. Libby P. Mechanisms of acute coronary syndromes and their implications for therapy. The New England journal of medicine. 2013; 368:2004–13. [PubMed: 23697515]
2. Virmani R, Burke AP, Farb A, Kolodgie FD. Pathology of the vulnerable plaque. J Am Coll Cardiol. 2006; 47:C13–8. [PubMed: 16631505]
3. Libby P, Pasterkamp G. Requiem for the 'vulnerable plaque'. European heart journal. 2015; 36:2984–7. [PubMed: 26206212]
4. Gimbrone MA Jr, Garcia-Cardena G. Endothelial Cell Dysfunction and the Pathobiology of Atherosclerosis. Circ Res. 2016; 118:620–36. [PubMed: 26892962]
5. Phinikaridou A, Hallock KJ, Qiao Y, Hamilton JA. A robust rabbit model of human atherosclerosis and atherothrombosis. Journal of lipid research. 2009; 50:787–97. [PubMed: 19141434]
6. Phinikaridou A, Ruberg FL, Hallock KJ, Qiao Y, Hua N, Viereck J, Hamilton JA. In vivo detection of vulnerable atherosclerotic plaque by MRI in a rabbit model. Circulation Cardiovascular imaging. 2010; 3:323–32. [PubMed: 20194634]
7. Abela OG, Ahsan CH, Alreefi F, Salehi N, Baig I, Janoudi A, Abela GS. Plaque Rupture and Thrombosis: the Value of the Atherosclerotic Rabbit Model in Defining the Mechanism. Curr Atheroscler Rep. 2016; 18:29. [PubMed: 27091328]
8. Phinikaridou A, Andia ME, Protti A, Indermuehle A, Shah A, Smith A, Warley A, Botnar RM. Noninvasive magnetic resonance imaging evaluation of endothelial permeability in murine atherosclerosis using an albumin-binding contrast agent. Circulation. 2012; 126:707–19. [PubMed: 22753191]
9. Jaffer FA, Calfon MA, Rosenthal A, Mallas G, Razansky RN, Mauskapf A, Weissleder R, Libby P, Ntziachristos V. Two-dimensional intravascular near-infrared fluorescence molecular imaging of inflammation in atherosclerosis and stent-induced vascular injury. Journal of the American College of Cardiology. 2011; 57:2516–26. [PubMed: 21679853]
10. Osborn EA, Jaffer FA. The year in molecular imaging. JACC Cardiovascular imaging. 2010; 3:1181–95. [PubMed: 21071007]
11. Morishige K, Kacher DF, Libby P, Josephson L, Ganz P, Weissleder R, Aikawa M. High-resolution magnetic resonance imaging enhanced with superparamagnetic nanoparticles measures macrophage burden in atherosclerosis. Circulation. 2010; 122:1707–15. [PubMed: 20937980]
12. Tang TY, Howarth SP, Miller SR, Graves MJ, Patterson AJ, JM UK-I, Li ZY, Walsh SR, Brown AP, Kirkpatrick PJ, Warburton EA, Hayes PD, Varty K, Boyle JR, Gaunt ME, Zalewski A, Gillard JH. The ATHEROMA (Atorvastatin Therapy: Effects on Reduction of Macrophage Activity) Study. Evaluation using ultrasmall superparamagnetic iron oxide-enhanced magnetic resonance imaging in carotid disease. Journal of the American College of Cardiology. 2009; 53:2039–50. [PubMed: 19477353]
13. Tang TY, Muller KH, Graves MJ, Li ZY, Walsh SR, Young V, Sadat U, Howarth SP, Gillard JH. Iron oxide particles for atheroma imaging. Arteriosclerosis, thrombosis, and vascular biology. 2009; 29:1001–8.
14. Jaffer FA, Vinegoni C, John MC, Aikawa E, Gold HK, Finn AV, Ntziachristos V, Libby P, Weissleder R. Real-time catheter molecular sensing of inflammation in proteolytically active atherosclerosis. Circulation. 2008; 118:1802–9. [PubMed: 18852366]
15. Verjans JW, Osborn EA, Ughi GJ, Calfon Press MA, Hamidi E, Antoniadis AP, Papafaklis MI, Conrad MF, Libby P, Stone PH, Cambria RP, Tearney GJ, Jaffer FA. Targeted Near-Infrared Fluorescence Imaging of Atherosclerosis: Clinical and Intracoronary Evaluation of Indocyanine Green. JACC Cardiovascular imaging. 2016; 9:1087–95. [PubMed: 27544892]
16. Vinegoni C, Botnaru I, Aikawa E, Calfon MA, Iwamoto Y, Folco EJ, Ntziachristos V, Weissleder R, Libby P, Jaffer FA. Indocyanine green enables near-infrared fluorescence imaging of lipid-rich, inflamed atherosclerotic plaques. Science translational medicine. 2011; 3 84ra45.
17. Kooi ME, Cappendijk VC, Cleutjens KB, Kessels AG, Kitslaar PJ, Borgers M, Frederik PM, Daemen MJ, van Engelshoven JM. Accumulation of ultrasmall superparamagnetic particles of iron oxide in human atherosclerotic plaques can be detected by in vivo magnetic resonance imaging. Circulation. 2003; 107:2453–8. [PubMed: 12719280]

18. Trivedi RA, U. King-Im JM, Graves MJ, Kirkpatrick PJ, Gillard JH. Noninvasive imaging of carotid plaque inflammation. Neurology. 2004; 63:187–8. [PubMed: 15249641]
19. Cui J, Kessinger CW, McCarthy JR, Sosnovik DE, Libby P, Thadhani RI, Jaffer FA. In vivo nanoparticle assessment of pathological endothelium predicts the development of inflow stenosis in murine arteriovenous fistula. Arteriosclerosis, thrombosis, and vascular biology. 2015; 35:189–96.
20. Jaffer FA, Verjans JW. Molecular imaging of atherosclerosis: clinical state-of-the-art. Heart. 2014; 100:1469–77. [PubMed: 24365664]
21. Mulder WJ, Jaffer FA, Fayad ZA, Nahrendorf M. Imaging and nanomedicine in inflammatory atherosclerosis. Science translational medicine. 2014; 6 239sr1.
22. Bourantas CV, Jaffer FA, Gijsen FJ, van Soest G, Madden SP, Courtney BK, Fard AM, Tenekecioglu E, Zeng Y, van der Steen AF, Emelianov S, Muller J, Stone PH, Marcu L, Tearney GJ, Serruys PW. Hybrid intravascular imaging: recent advances, technical considerations, and current applications in the study of plaque pathophysiology. European heart journal. 2016; 38:400–412.
23. Jaffer FA, Nahrendorf M, Sosnovik D, Kelly KA, Aikawa E, Weissleder R. Cellular Imaging of Inflainination in Atherosclerosis Using Magnetofluorescent Nanomaterials. Molecular Imaging. 2006; 4:85–92.
24. Ruehm SG, Corot C, Vogt P, Kolb S, Debatin JF. Magnetic resonance imaging of atherosclerotic plaque with ultrasmall superparamagnetic particles of iron oxide in hyperlipidemic rabbits. Circulation. 2001; 103:415–22. [PubMed: 11157694]
25. Hyafil F, Laissy JP, Mazighi M, Tchetche D, Louedec L, Adle-Biassette H, Chillon S, Henin D, Jacob MP, Letourneur D, Feldman LJ. Ferumoxtran-10-enhanced MRI of the hypercholesterolemic rabbit aorta: relationship between signal loss and macrophage infiltration. Arteriosclerosis, thrombosis, and vascular biology. 2006; 26:176–81.
26. Doran AC, Meller N, McNamara CA. Role of smooth muscle cells in the initiation and early progression of atherosclerosis. Arteriosclerosis, thrombosis, and vascular biology. 2008; 28:812–9.
27. Lim S, Lee SY, Seo HH, Ham O, Lee C, Park JH, Lee J, Seung M, Yun I, Han SM, Lee S, Choi E, Hwang KC. Regulation of mitochondrial morphology by positive feedback interaction between PKCdelta and Drp1 in vascular smooth muscle cell. Journal of cellular biochemistry. 2015; 116:648–60. [PubMed: 25399916]
28. Wall VZ, Bornfeldt KE. Arterial smooth muscle. Arteriosclerosis, thrombosis, and vascular biology. 2014; 34:2175–9.
29. Lim S, Park S. Role of vascular smooth muscle cell in the inflammation of atherosclerosis. BMB reports. 2014; 47:1–7. [PubMed: 24388105]
30. Hansson GK, Jonasson L, Holm J, Claesson-Welsh L. Class II MHC antigen expression in the atherosclerotic plaque: smooth muscle cells express HLA-DR, HLA-DQ and the invariant gamma chain. Clinical and experimental immunology. 1986; 64:261–8. [PubMed: 3527502]
31. Wilcox JN, Smith KM, Schwartz SM, Gordon D. Localization of tissue factor in the normal vessel wall and in the atherosclerotic plaque. Proceedings of the National Academy of Sciences of the United States of America. 1989; 86:2839–43. [PubMed: 2704749]
32. Drake TA, Morrissey JH, Edgington TS. Selective cellular expression of tissue factor in human tissues. Implications for disorders of hemostasis and thrombosis. The American journal of pathology. 1989; 134:1087–97. [PubMed: 2719077]
33. Schonbeck U, Mach F, Sukhova GK, Herman M, Graber P, Kehry MR, Libby P. CD40 ligation induces tissue factor expression in human vascular smooth muscle cells. The American journal of pathology. 2000; 156:7–14. [PubMed: 10623647]
34. Yancy AD, Olzinski AR, Hu TC, Lenhard SC, Aravindhan K, Gruver SM, Jacobs PM, Willette RN, Jucker BM. Differential uptake of ferumoxtran-10 and ferumoxytol, ultrasmall superparamagnetic iron oxide contrast agents in rabbit: critical determinants of atherosclerotic plaque labeling. Journal of Magnetic Resonance Imaging. 2005; 21:432–42. [PubMed: 15779033]
35. Litovsky S, Madjid M, Zarrabi A, Casscells SW, Willerson JT, Naghavi M. Superparamagnetic iron oxide-based method for quantifying recruitment of monocytes to mouse atherosclerotic lesions in

vivo: enhancement by tissue necrosis factor-alpha, interleukin-1beta, and interferon-gamma. Circulation. 2003; 107:1545–9. [PubMed: 12654614]

36. Schmitz SA, Coupland SE, Gust R, Winterhalter S, Wagner S, Kriesse M, Seamler W, Wolf K-J. Superparamagnetic Iron Oxide-Enhanced MRI of Atherosclerotic Plaques in Watanabe Hereditable Hyperlipidemic Rabbits. Investigative Radiology. 2000; 35:460–471. [PubMed: 10946973]
37. Kobayashi H, Watanabe R, Choyke PL. Improving conventional enhanced permeability and retention (EPR) effects; what is the appropriate target? Theranostics. 2013; 4:81–9. [PubMed: 24396516]
38. Sadat U, Jaffer FA, van Zandvoort MA, Nicholls SJ, Ribatti D, Gillard JH. Inflammation and neovascularization intertwined in atherosclerosis: imaging of structural and molecular imaging targets. Circulation. 2014; 130:786–94. [PubMed: 25156914]
39. Ibrahim T, Makowski MR, Jankauskas A, Maintz D, Karch M, Schachoff S, Manning WJ, Schomig A, Schwaiger M, Botnar RM. Serial contrast-enhanced cardiac magnetic resonance imaging demonstrates regression of hyperenhancement within the coronary artery wall in patients after acute myocardial infarction. JACC Cardiovascular imaging. 2009; 2:580–8. [PubMed: 19442944]
40. Kerwin WS, O'Brien KD, Ferguson MS, Polissar N, Hatsukami TS, Yuan C. Inflammation in carotid atherosclerotic plaque: a dynamic contrast-enhanced MR imaging study. Radiology. 2006; 241:459–68. [PubMed: 16966482]
41. Osborn EA, Jaffer FA. The advancing clinical impact of molecular imaging in CVD. JACC Cardiovascular imaging. 2013; 6:1327–41. [PubMed: 24332285]
42. Ughi GJ, Wang H, Gerbaud E, Gardecki JA, Fard AM, Hamidi E, Vacas-Jacques P, Rosenberg M, Jaffer FA, Tearney GJ. Clinical Characterization of Coronary Atherosclerosis With Dual-Modality OCT and Near-Infrared Autofluorescence Imaging. JACC Cardiovascular imaging. 2016; 9:1304–1314. [PubMed: 26971006]
43. Hara T, Ughi GJ, McCarthy JR, Erdem SS, Mauskapf A, Lyon SC, Fard AM, Edelman ER, Tearney GJ, Jaffer FA. Intravascular fibrin molecular imaging improves the detection of unhealed stents assessed by optical coherence tomography in vivo. European heart journal. 2017; 38:447–455.
44. Whitley MJ, Cardona DM, Lazarides AL, Spasojevic I, Ferrer JM, Cahill J, Lee CL, Snuderl M, Blazer DG 3rd, Hwang ES, Greenup RA, Mosca PJ, Mito JK, Cuneo KC, Larrier NA, O'Reilly EK, Riedel RF, Eward WC, Strasfeld DB, Fukumura D, Jain RK, Lee WD, Griffith LG, Bawendi MG, Kirsch DG, Brigman BE. A mouse-human phase 1 co-clinical trial of a protease-activated fluorescent probe for imaging cancer. Science translational medicine. 2016; 8 320ra4.
45. Phinikaridou A, Qiao Y, Giordano N, Hamilton JA. Detection of thrombus size and protein content by ex vivo magnetization transfer and diffusion weighted MRI. J Cardiovasc Magn Reson. 2012; 14:45. [PubMed: 22731842]
46. Yamashita A, Asada Y. A rabbit model of thrombosis on atherosclerotic lesions. J Biomed Biotechnol. 2011; 2011:424929. [PubMed: 21253503]
47. Yamashita A, Zhao Y, Zhao S, Matsuura Y, Sugita C, Iwakiri T, Okuyama N, Ohe K, Koshimoto C, Kawai K, Tamaki N, Kuge Y, Asada Y. Arterial (18)F-fluorodeoxyglucose uptake reflects balloon catheter-induced thrombus formation and tissue factor expression via nuclear factor-kappaB in rabbit atherosclerotic lesions. Circulation Journal. 2013; 77:2626–35. [PubMed: 23832535]
48. Shiomi M, Ishida T, Kobayashi T, Nitta N, Sonoda A, Yamada S, Koike T, Kuniyoshi N, Murata K, Hirata K, Ito T, Libby P. Vasospasm of atherosclerotic coronary arteries precipitates acute ischemic myocardial damage in myocardial infarction-prone strain of the Watanabe heritable hyperlipidemic rabbits. Arteriosclerosis, thrombosis, and vascular biology. 2013; 33:2518–23.
49. Yoo H, Kim JW, Shishkov M, Namati E, Morse T, Shubochkin R, McCarthy JR, Ntziachristos V, Bouma BE, Jaffer FA, Tearney GJ. Intra-arterial catheter for simultaneous microstructural and molecular imaging in vivo. Nature medicine. 2011; 17:1680–4.

Clinical Perspective

The majority of acute coronary syndromes result from focal thrombosis arising from atherosclerosis. The mechanisms underlying plaque thrombosis have evolved from a unique focus on disruption of a thin fibrous cap to also incorporate superficial plaque erosion, an entity more prevalent in smokers and younger women. These two etiologies of atherothrombosis share a common pathobiology involving diseased endothelial cells, and therefore approaches to understand impaired endothelial function in vivo could provide new mechanistic and predictive insights into atherothrombosis. In this experimental atherothrombosis study, we investigated in vivo mechanisms of impaired endothelial function using the engineered near-infrared fluorescence (NIRF) iron oxide nanoparticle CLIO-CyAm7. Following intravenous injection of nanoparticles into atheroma-bearing rabbits, NIR fluorescence microscopy demonstrated that CLIO-CyAm7 nanoparticles localized in the superficial intima as well as regions of plaque neovascularization, and further accumulated in multiple atheroma cell types, including macrophages, endothelial cells and smooth muscle cells. Co-injection of Evans Blue dye moreover revealed that CLIO-CyAm7 deposited in areas of impaired endothelial barrier function. In rabbits subjected to a modified Constantinides' model of triggered atherothrombosis, thrombosed plaques exhibited significantly higher CLIO-CyAm7 accumulation than non-thrombosed plaques. Finally, intravascular NIRF imaging, a high-resolution translatable molecular imaging approach for coronary artery disease, detected nanoparticles in atheroma in vivo ($p<0.05$ vs reference segments). The overall results provide new evidence that iron oxide nanoparticles report on plaque cells resident in areas of impaired endothelial barrier function, and that intravascular NIRF molecular imaging may provide a translatable approach to mechanistically investigate and predict atherothrombosis.

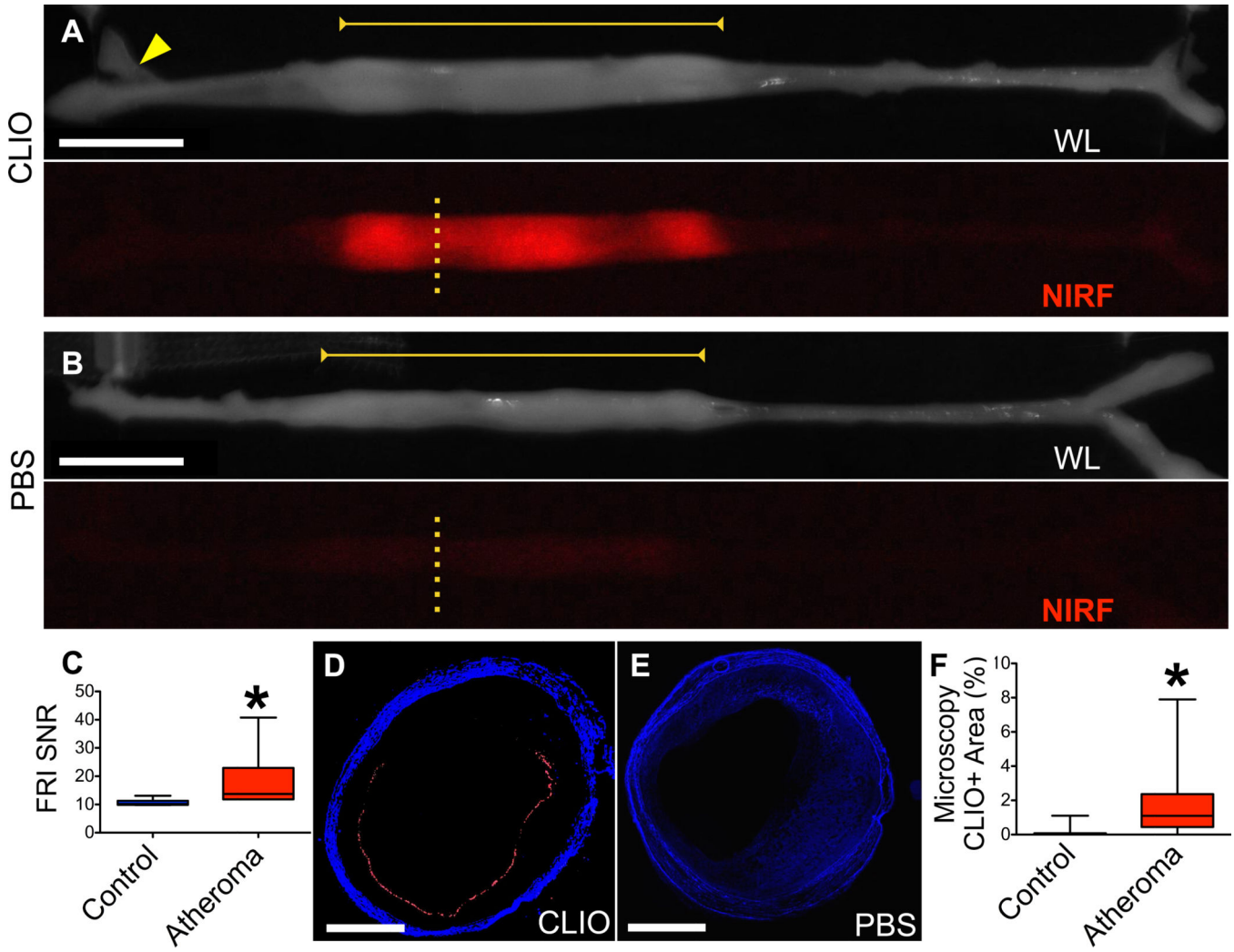

Figure 1. Ex vivo assessment of NIRF nanoparticle deposition in atheroma

(A) Representative *ex vivo* fluorescence reflectance imaging (FRI) in a rabbit 24 hours after CLIO-CyAm7 injection. White light (WL) image shows the resected aorta, stretched to premortem length determined by in vivo x-ray angiography. CLIO-CyAm7 signal evolved in atheroma (yellow bar) in contrast to minimal signal in the uninjured aorta, iliac bifurcation, or renal artery (yellow arrow). (B) *Ex vivo* FRI of a rabbit injected with PBS as a control exhibits minimal NIRF signal in atheroma (yellow bar). (C) Quantification of FRI signal in untriggered animals (n=6) showing significantly higher CLIO-CyAm7 signal in regions of atheroma compared to control renal artery (p=0.03). (D) Corresponding fluorescence microscopy (FM, yellow dashed line Figure 1A) of CLIO-CyAm7-injected atheroma showing luminal surface CLIO-CyAm7 signal (red) non-circumferentially distributed. (E) FM of a control atheroma (PBS injection, yellow dashed line Figure 1B) showing minimal CLIO-CyAm7 signal despite substantial atheroma detectable by autofluorescence. (F) FM analysis of percent positive CLIO-CyAm7 pixels in experimental, triggered rabbits at 48 hours showing increased CLIO-CyAm7 accumulation in regions of atheroma versus

uninjured aorta without evidence of intimal thickening ($p<0.0001$, n=183 slices). Scale bars; FRI = 1cm, Microscopy = 1mm. CLIO-CyAm7 = red, Autofluorescence = blue.

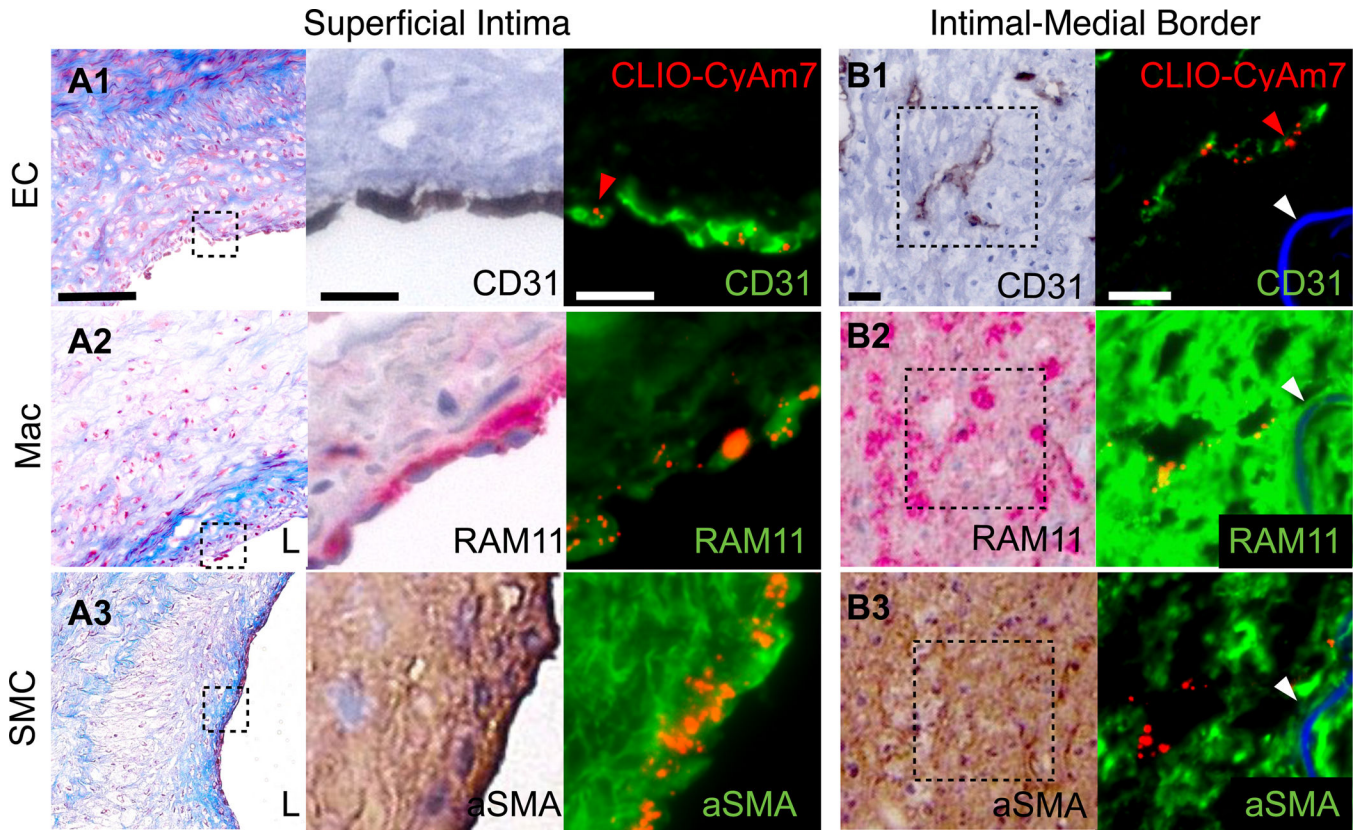

Figure 2. Cellular distribution of CLIO-CyAm7 nanoparticles in atherosclerosis

CLIO-CyAm7 uptake by plaque endothelial cells (ECs), macrophages (Macs) and smooth muscle cells (SMCs). Carstairs' stain shows structural characteristics of atheroma, including collagen (blue). (A) Carstairs', immunohistochemical (IHC), and immunofluorescence (IF) stains for CD31 (A1), RAM11 (A2), and alpha-smooth muscle actin (aSMA, A3) show correspondence between CLIO-CyAm7 signal (indicated by red arrows) and superficial, luminal ECs, macrophages, and SMCs, respectively. (B) Distribution of CLIO-CyAm7 along the intimal-medial border in regions of neovasculature as detected by CD31 stain (B1). CLIO-CyAm7 deposition occurred in areas of RAM11+ macrophages flanking the neovasculature (B2). IHC: RAM11+ = red; CD31+ and aSMA+ = brown. FM fusion images: CLIO-CyAm7 = red, IF antibodies = green, autofluorescence = blue. White arrows = internal elastic membrane. Scale bars: Low magnification Carstairs' = 100μm, IF and IHC = 25μm. L=vessel lumen.

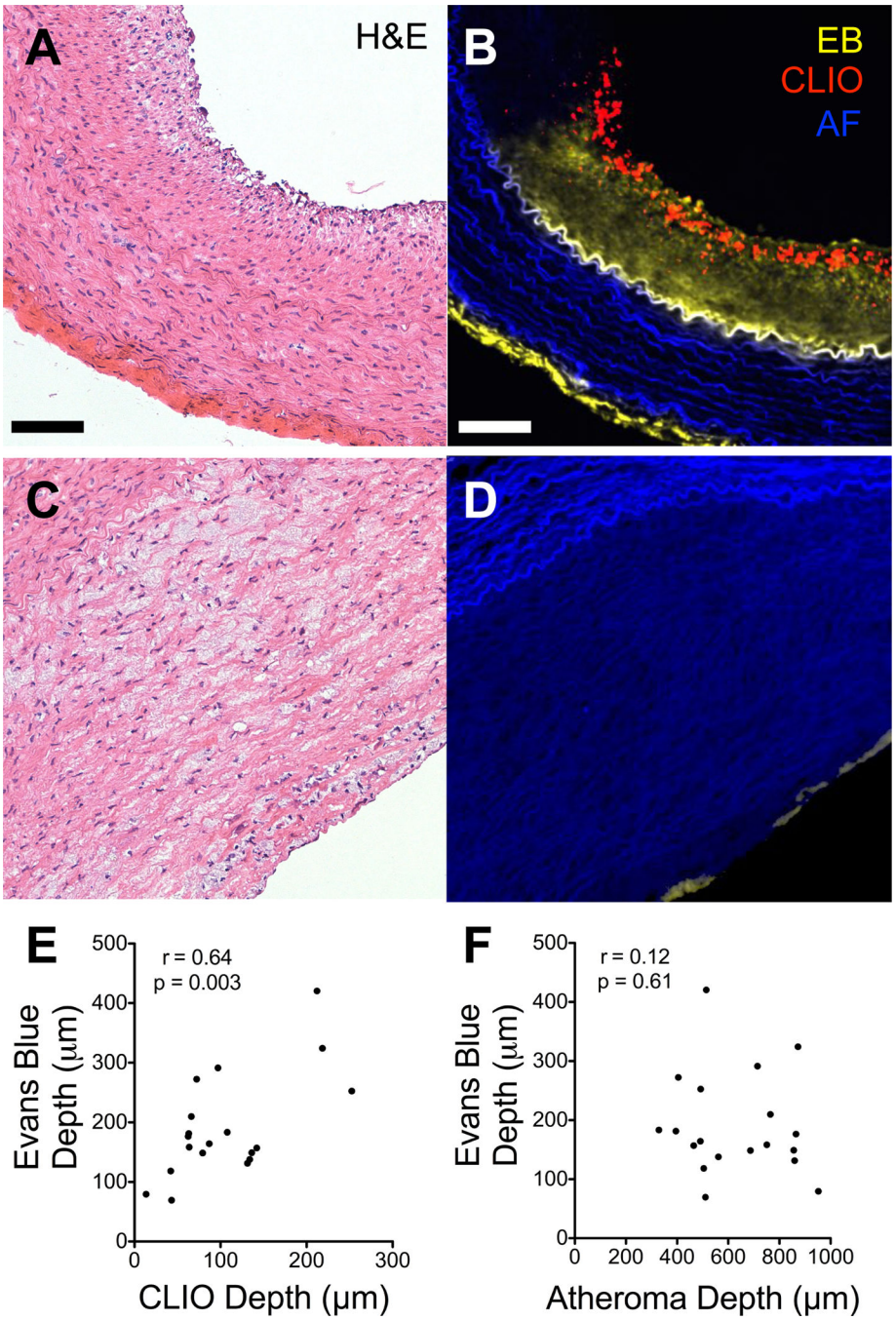

Figure 3. Plaque endothelial permeability assessed with Evans Blue concomitantly with CLIO-CyAm7 nanoparticle deposition

A subgroup of rabbits injected with CLIO-CyAm7 also received Evans Blue shortly prior to sacrifice. (A) Atheroma with extensive Evans blue uptake (yellow) throughout the intima limited peripherally by the internal elastic membrane (autofluorescence, blue). CLIO-CyAm7 (red) similarly penetrates below the endothelial layer throughout the intima. (B) Atheroma with minimal, superficial Evans blue uptake and minimal CLIO-CyAm7 signal. (C) Evans Blue and CLIO-CyAm7 depths of penetration correlated strongly (r=0.64,

p=0.003, n=19). (D) Weak correlation between the depth of Evans Blue penetration and plaque thickness (r=0.14, p=0.61, n=19). Scale bar 100μm.

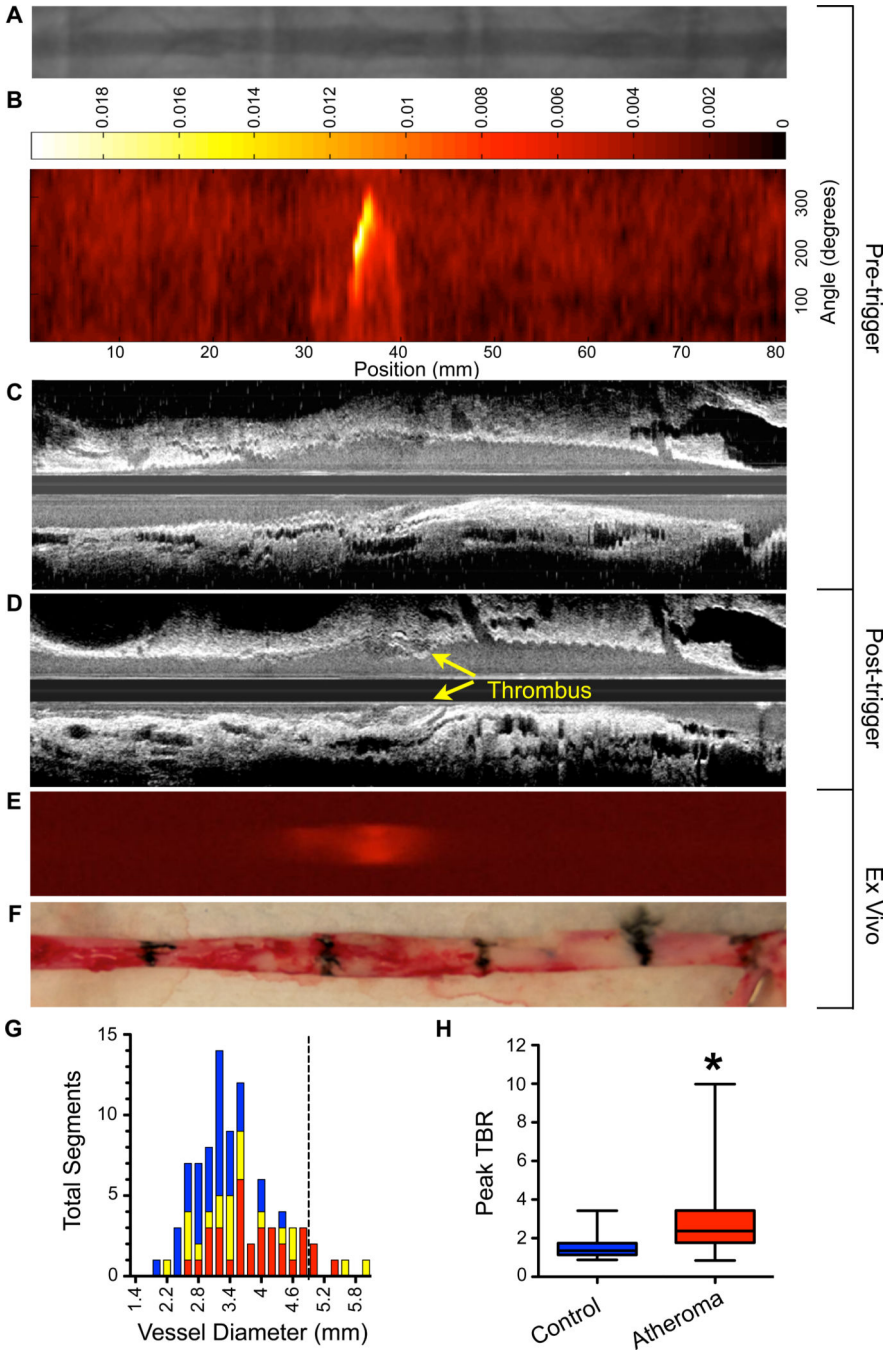

Figure 4. *In vivo* and *ex vivo* NIRF imaging of atherothrombosis

Rabbits underwent the protocol described in Supplemental Figure 1. (A) Pre-trigger x-ray angiography showing the aorta for image co-registration (not shown are the iliac bifurcation and renal artery). (B) Pre-trigger *in vivo* NIRF imaging projected into a 2D matrix of translational distance (x-axis) and 0–360 degree of rotation (y-axis). (C,D) Pre- and post-trigger IVUS imaging showing triggered luminal thrombus (yellow arrows) corresponding to the region of increased NIRF signal intensity on pre-trigger NIRF imaging in (B). (E) *Ex vivo* FRI of CLIO-CyAm7 corroborating *in vivo* 2D NIRF imaging. (F) Gross pathology of

the resected aorta with 1.5cm black tissue markings for histological analysis and co-registration with *in vivo* imaging above. (G) Histogram of vessel diameter measured by cross sectional IVUS imaging. Red indicates atheroma without attached thrombus, yellow indicates atheroma with attached thrombus and blue indicates uninjured control aortic segments. The dashed line indicates the 5mm cutoff for exclusion of NIRF imaging data due to distance attenuation of the NIRF signal in large vessels. (H) *In vivo* 2D NIRF imaging showed significantly higher TBR in areas with atheroma, compared to uninjured segments of the aorta (peak TBR 2.86±1.82 and 1.55±0.65, p=0.001).

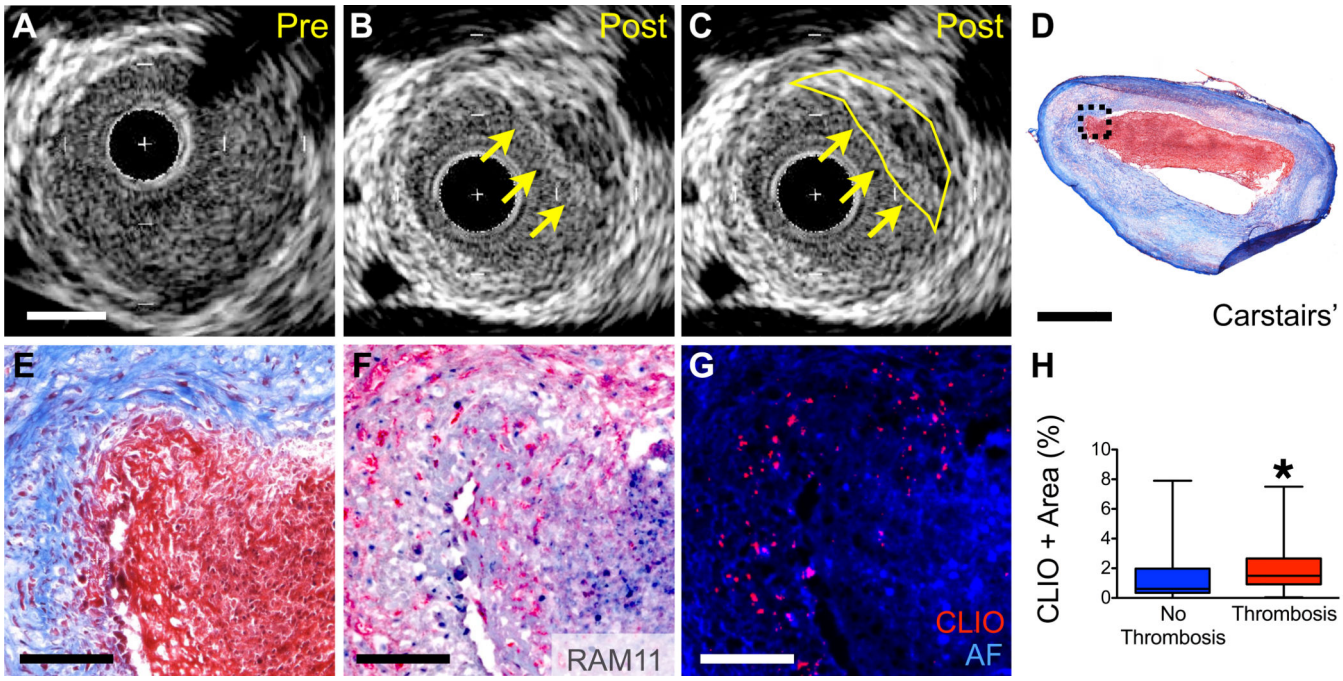

Figure 5. In vivo and microscopic analyses of nanoparticle deposition and triggered plaque thrombosis

(A) Cross sectional IVUS image of rabbit aorta with atheroma prior to pharmacologic triggering. (B,C) Post-triggering IVUS image corresponding to (A) demonstrating new luminal irregularity (yellow arrows and outline) consistent with new thrombus (segmented in (C)). (D,E) Corresponding histology of plaque with adherent thrombus. Carstairs' staining of fibrin rich adherent thrombus (red). (F) RAM11+ macrophages are present at the surface below the thrombus. (G) Epifluorescence microscopy revealing increased CLIO-CyAm7 (red) at the plaque shoulder and underlying areas of thrombus. (H) Significantly higher CLIO-CyAm7 accumulation occurred in regions with thrombosis compared to atheroma without thrombosis (2.1±1.7%, n=34, and 1.5±1.9%, n=23, respectively, p=0.045). Scale bars: IVUS and low magnification histology = 1mm, high magnification histology = 100μm.